SAE INTERNATIONAL®

# Combining Modeling Methods to Accurately Predict Wind Noise Contribution

2015-01-2326
Published 06/15/2015

**Denis Blanchet and Anton Golota**
ESI Group

**CITATION:** Blanchet, D. and Golota, A., "Combining Modeling Methods to Accurately Predict Wind Noise Contribution," SAE Technical Paper 2015-01-2326, 2015, doi:10.4271/2015-01-2326.



## Abstract

Recent developments in the prediction of the contribution of wind noise to the interior SPL have opened a realm of new possibilities. The main physical mechanisms related to noise generation within a turbulent flow and the vibro-acoustic transmission through the vehicle greenhouse is nowadays better understood. Several simulation methods such as CFD, FEM, BEM, FE/SEA Coupled and SEA can be coupled together to represent the physical phenomena involved. The main objective being to properly represent the convective and acoustic component within the turbulent flow to ensure proper computation of the wind noise contribution to the interior SPL of a vehicle. This paper introduces the reader to the various physical mechanisms involved in wind noise, it also describes the most common ways of characterizing the source and representing the transmission paths to the interior and finally it presents the validation of a vehicle vibro-acoustic model before presenting the correlation between simulations results and measurements for the case with and without mirror.

## Introduction

In order to model wind noise it is necessary to understand the source, the paths which typically involve direct vibro-acoustic transmission through certain regions of the structure, transmission through nearby leaks/seals and isolation and absorption provided by the interior sound package and the receiver and in particular, the frequency range(s) in which wind noise provides an audible contribution to the interior noise in the occupant's ears. While many regions of a vehicle can contribute to wind noise, the fluctuating surface pressures on the front side glass due to vortices and separated flow generated by the A-pillar and mirror are often an important contributor.

This paper presents an overview of different approaches that can be used to efficiently predict wind noise contribution to overall SPL at the driver's ear. After describing the physical phenomena involved in wind noise simulation, a review of major wind noise source characterization will be presented. Following is a description of vibro-acoustics methods used to predict interior SPL for a given wind noise source model. Topics such as availability of source data, model building and computation time as factors guiding selection of an approach that ensures getting the right model at the right time are then discussed. Finally, validation cases for both vibro-acoustics (VA) and Aero-Vibro-Acoustics (AVA) are presented.

## From Turbulent Flow to Vehicle Interior SPL

### *Physical Phenomena Involved*

A turbulent flow generated outside a vehicle contains both a convective and an acoustic pressure fluctuations component on side glass (Figure 1). This energy can potentially be transmitted to the interior of a vehicle and be detrimental to the sound quality experienced by occupants.

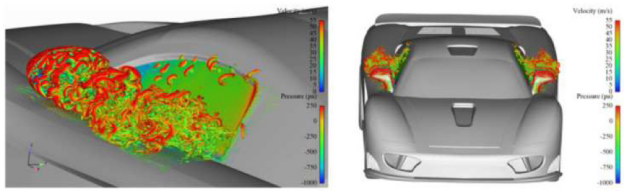

Figure 1. CFD turbulent flow generated behind side mirror and A-pillar (Source: OpenFoam-ESI Group)

The following sections describe the main noise generation principles involved in wind noise.

#### Pressure Fluctuation on Side Glass

The turbulent flow outside a vehicle generates a fluctuating surface pressure field on the side glass which includes a convective and an acoustic component. The convective component is related to the pressure field generated by eddies travelling at the convection speed. The acoustic component is related to acoustic waves travelling within the flow and being generated on various surfaces before reaching the side glass. The acoustic component is typically very small in amplitude compared to the convective component and as will be shown later in this paper, can be the major contributor at coincidence

frequency of the side glass. Furthermore, the acoustic waves reaching the side glass are highly directional. Both the convective and the acoustic components contribute to the sound pressure level (SPL) at the driver's ear (Figure 2).

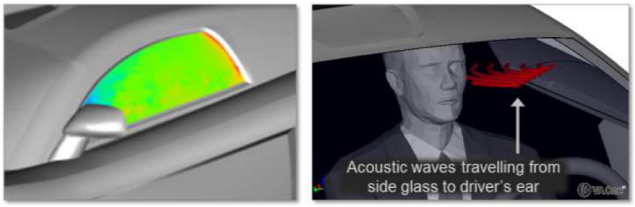


Figure 2. Left: CFD fluctuating surface pressure on side glass. Right: sketch of acoustic waves propagating from side glass to the driver's ear.

### Pressure Fluctuation on Mirror and A-Pillar

In Figure 3 on the left side, the flow velocity is the highest in the front of the side mirror. It is also the location of lowest fluctuation. The flow in front of the mirror is steady as opposed to the rear face of the mirror where the flow fluctuates the most. The eddies tapping the rear face of the mirror create acoustic waves that travel rearward towards the side glass with a specific heading. This source term is associated to a dipole source (surface terms). The acoustic waves travelling towards the side glass are likely to be transmitted inside the vehicle through the side glass and to the driver's ear as illustrated in Figure 3 on the right.

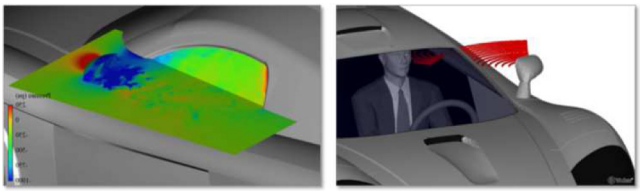

Figure 3. Left: CFD velocity field around on side mirror. Right: sketch of acoustic waves propagating from side mirror to the driver's ear (right).

### Acoustic Sources within Eddies

Eddies within the turbulent flow can also generate noise and therefore constitute acoustic sources. These sources act as quadrupole acoustic sources and are referred to as volume source terms. These acoustic sources are at close proximity to the side glass however at automobile speeds, these source terms are considered negligible (Figure 4).

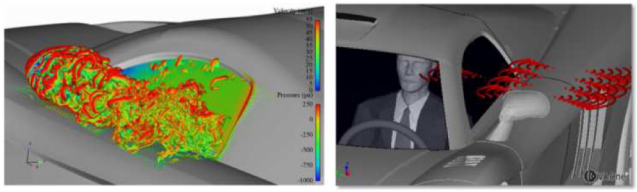

Figure 4. Left: CFD turbulent flow behind side mirror. Right: Sketch of acoustic waves propagating from turbulent flow to the driver's ear and away from vehicle.

### Pressure Fluctuation on Side Glass - Outward Effect

Pressure fluctuations on the side glass also generate acoustic waves that propagate away from the side glass. These waves can interfere with incoming acoustic waves from A-Pillar and mirror. It is believed to have a negligible impact on driver's ear SPL (Figure 5) [1].

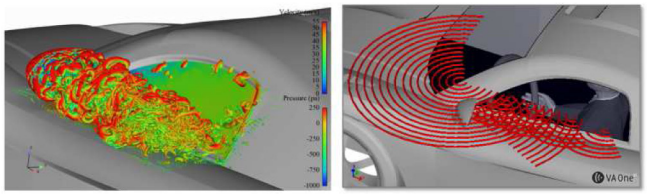

Figure 5. Left: CFD fluctuating surface pressure on side glass and velocity field around mirror and A-Pillar. Right: Sketch of acoustic waves travelling away from vehicle. These acoustic waves interfere with grazing incidence waves coming from side mirror and A-Pillar (right).

## *Overview of Available Approaches*

Several methods of representing the wind noise sources have been investigated over the past 10 years in the automotive industry. Empirical methods have shown their merits and limitations especially when the geometry of the structure changes significantly compared to previous computations [2,3,4,5]. A more predictive approach, based on the ability of coupling time domain turbulent flow data to a vibro-acoustics model has opened new possibilities. The computation process is illustrated in Figure 6.

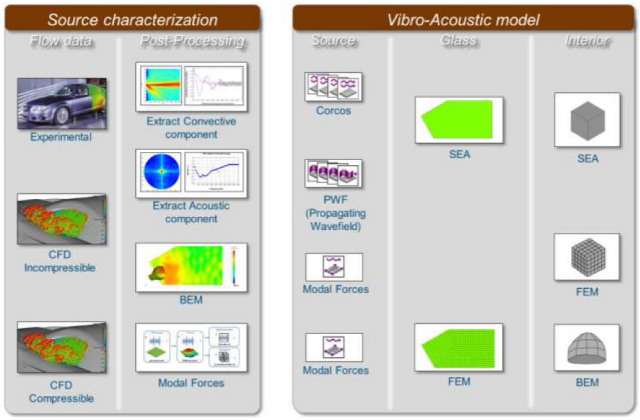


Figure 6. Illustration of source characterization (left) and vibro-acoustic modelling (right) approaches discussed in this paper

The left side of Figure 6 shows the source characterization topics that will be covered in the paper and the right side the vibro-acoustics methods that can be combined to compute the interior SPL. In this work, the combination of an aero-acoustic (CAA) sources model with a vibro-acoustic (VA) model is called an aero-vibro-acoustic (AVA) model.

### Turbulent Flow Data

The turbulent flow can be represented by measurement of the fluctuating surface pressure on the side glass. In theory, these nodal time domain pressures include the convective and the acoustic component. Care must be taken to ensure both components are well sampled and represented in the data. Typically, surface pressure measurement points should be close enough to sample the short convective wavelengths at higher frequency. The microphones should be small enough to avoid “microphone size effect” at higher frequency. This subject is out of scope of this paper and more information can be found here [4,6,7]. Turbulent flow can also be represented using CFD compressible simulation which includes both convective and acoustic components. If, on the other hand, results of an incompressible CFD simulation are available then only the

convective part will be represented by the CFD data since the fluid cannot transport the acoustic waves through compression and decompression of the fluid. In this case, the acoustic component can be computed using standard aero-acoustic analogies.

## Post-Processing

Before discussing the fluctuating surface pressures post-processing approaches, it is useful to first investigate how different loads are transmitted through a typical side glass. In particular, it is often found that the glass acts as a spatial filter and preferentially transmits certain wavenumbers found in the fluctuating surface pressure data [8,9,10]. The spatial filtering of different exterior fluctuating surface pressures can be demonstrated using a simple numerical example. Figure 7 shows three glass panels of dimension 1 m × 1 m × 3.5 mm. Each has a constant structural damping loss factor of 6% and is placed in contact with a 1 $m^3$ acoustic fluid.

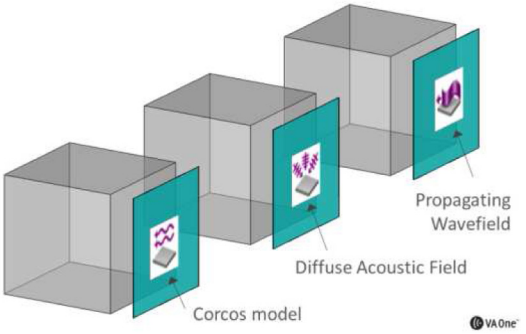


Figure 7. Glass panel of dimension 1 $m^2$ and thickness 3.5 mm in contact with a 1 $m^3$ acoustic cavity and excited by i) TBL (Turbulent Boundary Layer : Corcos model with a 40 m/s mean flow), ii) DAF (Diffuse Acoustic Field) and iii) PWF (Propagating Wave Field with directivity representing wave travelling from mirror).

A Turbulent Boundary Layer (TBL) based on Corcos model with a 40 m/s free stream velocity is applied to the first panel. A Diffuse Acoustic Field (DAF) representing waves having the same probability of impinging on the glass from any direction is applied to the second panel. Finally, a Propagating Wave Field (PWF) representing waves travelling with a specific heading as illustrated in Figure 8 is exciting the third panel.

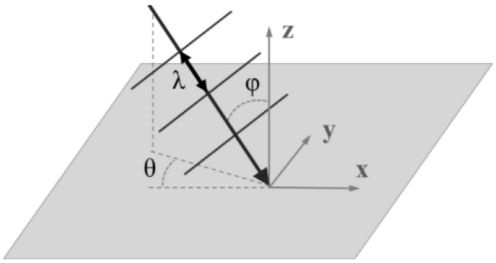


Figure 8. Propagating Wave Field incident angles description

An angle φ equal to 70° is used since it is close to the one found between a mirror rear face and a side glass normal vector. The magnitude of the exterior fluctuating surface pressure of each load has been normalized to have unit amplitude. An SEA model is then used to predict the interior sound pressure levels of each cavity [11]. It can be seen in Figure 9 that even though the loads have the same exterior fluctuating surface pressure amplitude, the interior sound pressure level due to the Turbulent Boundary Layer is approximately 30dB lower than that due to the DAF and 10 to 30 dB lower compared to the PWF due to the different spatial correlation characteristics of each load.

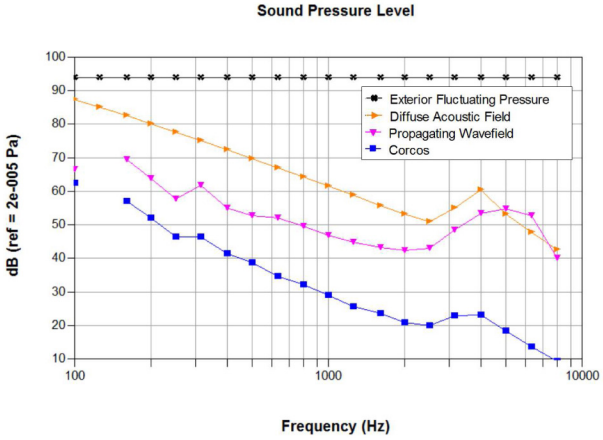


Figure 9. Exterior and interior Sound Pressure Level for three different loading.

The reason for the difference in acoustic fluid SPL is due to differences in the "spatial correlation" of the loads. The cross-spectra $\mathbf{S}_{pp}$ between two locations in a spatially homogenous fluctuating surface pressure can be written as

$$S_{pp}(x,x') = F(\omega)\,R(x,x',\omega) \tag{1}$$

where **F** is a function of frequency (that does not depend on location) and **R** represents a spatial correlation function. A diffuse acoustic field has a spatial correlation function **R** of the form [2]

$$R(x,x') = \sin(kr)/kr; \quad r = |x - x'| \tag{2}$$

where **k** is the acoustic wavenumber and **r** is the distance between two locations **x** and **x′** on the surface. A Turbulent Boundary Layer (modelled using a Corcos type model) has a spatial correlation function **R** of the form [13]

$$R(\Delta x,\Delta y) = \exp\left(-\alpha_x|\Delta x| - \alpha_y|\Delta y|\right)\exp\left(-ik_c\Delta x\right) \tag{3}$$

where $\Delta\mathbf{x}$ is the separation distance between two points in the flow direction, $\Delta\mathbf{y}$ is the separation distance in the cross flow direction, $\alpha\mathbf{x}$ and $\alpha\mathbf{y}$ are spatial correlation decay coefficients in the flow and cross-flow directions and $\mathbf{k}_c$ is the convection wavenumber.

For a side glass problem, the acoustic wavenumber is typically much lower than the convection wavenumber across much of the frequency range of interest (the DAF and PWF have a much longer spatial correlation length than the TBL source). The three different excitations therefore result in very different distributions of energy in wavenumber space, and this preferentially excites different structural mode shapes of the glass. The Diffuse Acoustic Field and Propagating Wave Field have a concentration of energy at low wavenumbers. Below glass coincidence, (peak in interior SPL around 4kHz is associated with the glass coincidence frequency) this typically excites the 'non-resonant' (mass controlled) modes of the glass. Since these

modes are also efficient acoustic radiators, the mass controlled modes are typically the dominant transmission path below coincidence. Above coincidence, the resonant modes become the dominant transmission path but these modes are also well excited by the wavenumber content of a DAF or PWF. In contrast, a Turbulent Boundary Layer typically has a concentration of energy at the convective wavenumber of the flow and has much smaller concentrations of energy at the wavenumbers associated with the resonant and mass controlled modes of the panel. The net result is that a DAF or PWF is transmitted through the glass much more efficiently than a Turbulent Boundary Layer for the same RMS fluctuating surface pressure. In summary, in order to characterize an exterior fluctuating surface pressure and enable design changes that would best impact interior noise, it is necessary to be able to characterize not only the magnitude of the fluctuating surface pressure but also its wavenumber content.

### *Extract Convective Component*

The convective component of a turbulent flow can be represented as a Corcos model. This empirical approach has been widely used in the past in the aerospace industry [10,13,14,15,16,17] and has recently been applied with success in the train and automotive industry for wind noise application [7,18,19,20,21]. A fundamental hypothesis of a Corcos model is that the turbulent flow should exhibit a spatially homogenous fluctuating surface pressure character on a surface. It has been observed that on a side glass surface three main regions have been identified: the mirror wake, the A-Pillar vortex and a reattached region. These regions typically exhibit very different flow characteristics and can be modelled using several Corcos sources with parameters corresponding to each flow region. These various sources can be applied to a single SEA panel for example. One can decide to use an average set of Corcos parameters representing the side glass in its entirety. In this case, a single TBL source would be applied on the side glass SEA panel.

The extraction of the Corcos parameters such as the spatial correlation decay coefficients in both flow and cross-flow direction and the convection wavenumber from the turbulent flow data is illustrated in Figure 10 and implemented in [11]. Step 1 shows the spatial distribution of the auto-spectra of pressure. Step 2 shows the normalized spatial correlation in flow (blue) and in cross-flow (red) direction with respect to nodal distance extracted from the turbulent flow data. The full cross-spectral matrix is calculated for a (dense) grid of points across the surface region of interest. A spatial averaging is performed by using bins in which nodes are grouped as illustrated in step 3. This surface region is divided into a coarser orthogonal grid and a reduced cross-spectral matrix is obtained by averaging the auto-spectra and cross-spectra within each cell of the coarse grid. Spatial correlation functions $R_{pp}$ are then obtained by averaging overall all pairs of cells with the same separation distance in the flow and cross-flow directions. In step 4, the log of the resulting cross-correlation function is used to extract the spatial correlation decay coefficient in flow and cross-flow direction. Finally, step 5 shows how the phase of the resulting cross-correlation function is used to extract the convective wavenumber.

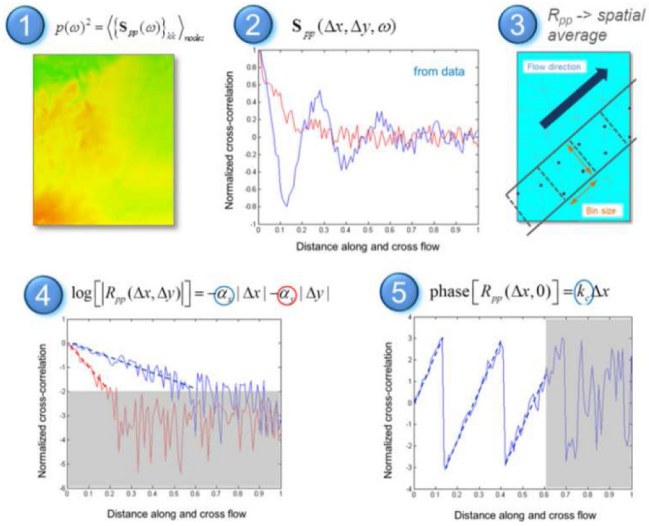


Figure 10. Extracting convective component from turbulent flow.

### *Extract Acoustic Component*

In the previous section, the spatial correlation function was presented with respect to distance between two points. Using a 1D wavenumber transform it is possible to visualize the spatial correlation function in terms of wavenumber content vs frequency (Figure 11).

$$P(X,t) \rightarrow P(X,\omega)) \rightarrow Rpp(\Delta x,\omega) \rightarrow Rpp(kx,\omega)$$
$$P(X,t) \rightarrow P(X,\omega)) \rightarrow Rpp(\Delta y,\omega) \rightarrow Rpp(ky,\omega)$$

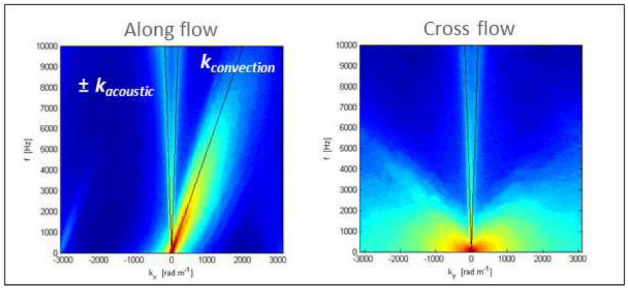


Figure 11. 1D wavenumber transform of turbulent flow surface pressure.

The wavenumber content in the flow and cross-flow direction can also be obtained by calculating the 2D wavenumber transform of the spatial correlation functions obtained in the previous section (at each frequency of interest). The magnitude of the 2D wavenumber transforms for two frequencies are plotted in Figure 11 (the scale of the contour plot is approximately 30 dB). The acoustic circle is shown in white in the figure, and the convection wavenumber for a 30 m/s flow is plotted as a straight line segment. It can be seen that at low frequencies, there are two distinct concentrations of energy in wavenumber space at the convective wavenumber and at acoustic wavenumbers. At higher frequencies, there is little evidence of any energy at the convective wavenumbers. This may be physical but it may also perhaps be an artifact of the CFD calculation.

Comparing Figure 10 step 1, Figure 11 and Figure 12, it can be seen that a complex distribution of energy in the spatial domain becomes a much simpler distribution of energy in the wavenumber domain (1D and 2D). It is possible to fit an equivalent acoustic source (DAF or PWF) to the CFD data by integrating the energy in the acoustic circle in wavenumber space. The RMS pressure spectrum for the total fluctuating surface pressure field and its acoustic component (DAF)

are shown in Figure 13. Below 350Hz there is less than one acoustic half wavelength across the dimension of the side glass and so there is not enough resolution in the wavenumber transform to provide a good estimate of the acoustic wavenumber content. However, for wind noise applications interest typically lies in higher frequency content and so this is not a significant constraint. It can be seen that the estimated amplitude of the acoustic component is 5-30dB less than the amplitude of the overall fluctuating surface pressure. However, since the glass is 30dB more sensitive to an acoustic component than to a convective component as previously shown, the acoustic component can often be one of the dominant contributors to interior noise.

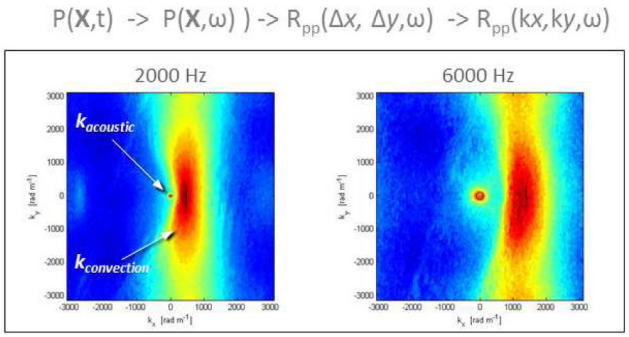


Figure 12. 2D wavenumber transform of turbulent flow surface pressure

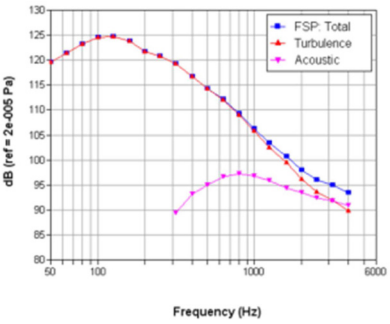


Figure 13. Turbulent flow total surface pressure (blue), convective part (red) and acoustic component (pink)

### *Using BEM to Propagate External Acoustics*

The Navier-Stokes equations are notoriously difficult to solve numerically, and a wide range of approximate strategies has been developed (LES, RANS, etc) to do so. In particular it is very difficult to solve for both turbulent flow and acoustic radiation at the same time, since turbulence is small scale and requires a very fine grid of computational mesh points and acoustic waves and sound radiation require a large spatial region to be modeled. Many CFD engineers avoid this problem by assuming that the flow is incompressible which removes the acoustics [22]. This section discusses how the acoustics can be added to an incompressible CFD simulation.

For wind noise automotive application, this means using BEM to propagate acoustic waves generated from the fluctuating surface pressure locations such as mirror and A-Pillar surfaces towards the side glass (see Figure 14)

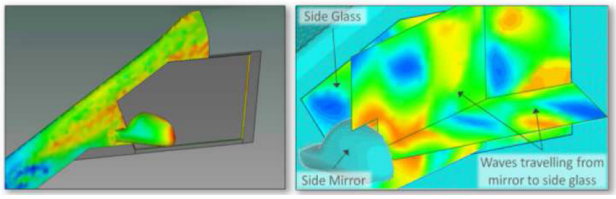


Figure 14. CFD fluctuating surface pressure imported on mirror and A-Pillar (left) applied as a boundary source term on a BEM model that propagates acoustic waves from mirror and A-Pillar to side glass

New derivation of the acoustic analogy based on Curle's integral version of the Lighthill equation for BEM allows the use of CFD incompressible analysis to model the turbulent flow [1]. CFD pressure time history data are then directly imported into [11] which uses this CFD data as a source for a BEM fluid and computes acoustic propagation and scattering. The use of time domain surface pressure data translates into small file sizes and fast calculations. This method is also less sensitive to mesh projections than other formulations using volume terms. The only restriction is that the near fields from quadrupole source terms are neglected. The theory behind this method is strictly valid for flows with low Mach numbers (Ma<0.3) where surface terms dominate. In addition to exterior wind noise modelling, this approach can also be used to model flow induced duct noise such as automotive HVAC systems.

In summary, the Curle's approach is used to split the original set of volume sources into a set of surface sources (dipoles) and a set of remaining volume sources (quadrupoles). The quadrupole volume sources are then neglected; this means that only the hydrodynamic pressure on the surface is needed for the analysis. In contrast (for example) a volume code does not apply Curle's approach and retains the original set of volume sources, thus requiring full hydrodynamic flow information for the acoustic solution.

### *Modal Forces*

When FEM is used to represent the side glass, one can directly use the time domain fluctuating surface pressure and convert them into modal forces. The process is illustrated in Figure 15.

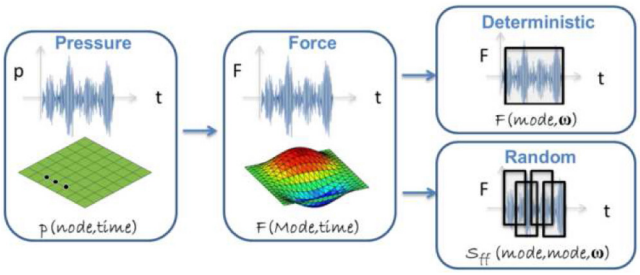


Figure 15. Using modal forces to represent forcing function from turbulent flow.

The time domain pressures are converted into forces and projected onto the modes of the side glass. The full time domain modal force signal is then either used in its entirety as a single window and used in the AVA model as a deterministic excitation or the time signal is post-processed and averaged using overlapping segments to generate a random source.

## Description of the Vibro-Acoustic (VA) Model

The vibro-acoustic model is composed of a source, a transfer path (the side glass in this study) and a receiver. This VA model offers the possibility to mix and match different VA methods depending on user requirements in terms of accuracy, computation time, time needed to build a model and source data availability.

### *Wind Noise Source Representation*

As previously described, a Corcos model can be used to represent the convective source term of a turbulent flow in a VA model. This source can be applied to a SEA or FEM panel. The Corcos parameters can be either extracted from measured data or from a CFD computation. The acoustic component of a turbulent flow can be represented by either a DAF or a PWF. These sources can be applied to a SEA or FEM panel. The amplitude of the pressure field can be either computed from a 2D wavenumber transform or a BEM computation where incompressible CFD data is used as boundary condition. Finally, modal forces can be used to project the fluctuating surface pressure onto the modes of a FEM panel. This approach can be used with data that contains both convective and acoustic component or it can be used with data containing only a single component. The latter permits the calculation of the contribution of each component separately.

### *Modelling the Side Glass*

The side glass can be either tempered or laminated. Several modelling approaches can be used to best represent the behavior of the glass and this is out of the scope of the present paper. Note that a side glass has typically a few hundred modes up to 5kHz and do not represent a large computation expense compared to the interior volume of the vehicle. Furthermore, the use of FEM allows the designer to test different boundary conditions and complex lamination to find the best possible design.

One can also use a SEA glass which permits a fast computation and a reliable prediction of the overall behavior of the glass especially at higher frequencies where the glass coincidence frequency contributes to increase the acoustic transparency of the glass. Laminated glass can also be modelled accurately using SEA and a 1D FEM model implemented in the general laminate module in [11].

### *Modelling Vehicle Interior*

The interior of a vehicle can be modelled as a SEA, a FEM or BEM fluid domain. The number of modes in the interior volume can be as high as 10 000 below 3 kHz for the structure studied (see Table 1). SEA models used to compute the response of such a volume can solve in a few minutes, where BEM might take a few days and FEM would be impractical to do in modal response. The advantage of a deterministic method such as BEM is that the response can be computed at specific microphone locations. SEA will provide the average SPL in a location such as the driver headspace. An important aspect of the interior volume is the localized absorption which will affect the way acoustic waves will travel in the volume.

Table 1. Mode count for SAE body interior cavity

| Frequency (Hz) | Mode count |
|---|---|
| 125 | 5 |
| 250 | 23 |
| 500 | 123 |
| 1000 | 770 |
| 2000 | 5340 |
| 4000 | 39246 |
| 8000 | 301012 |

Computing the wind noise contribution to total SPL at driver's ear can be quite simple if one only accounts for the transfer through the side glass. There is no need to create a full vehicle VA model, the interior fluid cavity with the right surface absorption is sufficient. Nonetheless, the final objective is usually to include the wind noise sources into a full vehicle model and make design changes that will either improve passengers experience or reduce sound package cost while maintaining the vibro-acoustic performance of the vehicle.

### *Approach Selection Based on Design Process Phase*

The adequate approach to select depends on many factors:

- Available turbulent flow data
- Available computation resources
- Available resource/time for model building
- Available time for computation
- Design process stage
- Required accuracy
- Absolute vs relative interior noise levels

The following sections illustrate several possible approaches and discuss the advantages and inconveniences of their use. Several variants are not covered by this paper and will have to be addressed at a later time. The selected approaches are organized based on the turbulent flow data availability and side glass modelling method.

## Experimental Wind Tunnel Flow Data Available

### *SEA Side Glass Approach*

When experimental wind tunnel test data are available, several approaches can be selected to predict interior vehicle SPL. Figure 16 shows the case where the convective and acoustic components are extracted and a SEA side glass is used in conjunction with either a SEA or a FEM interior fluid. This approach has the advantage of being very fast to compute and setup. Once both components of turbulent flow are extracted, the wind noise contribution to interior SPL is computed in minutes. The model setup is also fast, using either a single cavity model or a full vehicle coarse SEA model for target setting of different sub-assembly or a detailed full vehicle SEA model if one is available. Predictions are averaged over a volume around the passenger's head unless a FEM cavity is used, then a specific microphone location can be predicted.

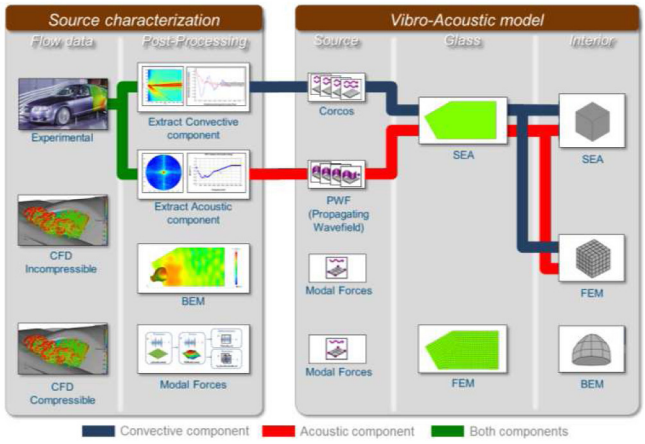


Figure 16. Using experimental wind tunnel data and a SEA or FE/SEA model to predict interior wind noise

Drawbacks to this approach are that a clay model or prototype is needed to perform wind tunnel test. To properly extract the convective component, the measurement locations have to be chosen adequately [7]. Finally, frequency domain of validity of the extracted convective component might be limited and well below the coincidence frequency of the side glass due to the number of modes in the FEM interior volume.

### *FEM Side Glass Approach*

Figure 17 shows the case where the modal forces are used to represent the turbulent flow and a FEM side glass is used in conjunction with a BEM, a FEM or SEA interior fluid. This approach has the advantage of being very accurate since the source data is taken as is, converted into modal forces, applied on a FEM panel and a deterministic interior fluid can be used. The model setup is simple and can be completed within a few hours. A SEA interior fluid cavity can also be used to increase frequency range of computation to higher frequencies than the glass coincidence and therefore reduce computation time.

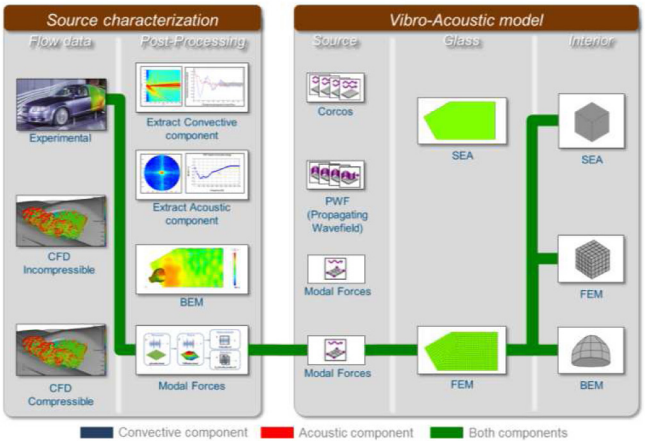


Figure 17. Using experimental wind tunnel data and a BEM or FEM or FE/SEA model to predict interior wind noise

Drawbacks to this approach are that a clay model or prototype is needed to perform wind tunnel test. To properly capture the convective component, the measurement locations have to be chosen adequately [7]. The contribution from the convective and acoustic component cannot be separately computed. Finally, frequency domain of validity of the convective component might be limited and well below the coincidence frequency of the side glass because of shorter correlation length as the frequency increases.

## CFD Incompressible Flow Data Available

### *SEA Side Glass Approach*

When CFD incompressible turbulent flow data are available, several approaches can be selected to predict interior vehicle SPL. Figure 18 shows the case where the convective component is extracted from the data to find the Corcos parameters. It also shows that the acoustic component is evaluated by means of a BEM model propagating the acoustic waves from the fluctuating surface pressure locations towards the side glass. Finally, a SEA side glass is used in conjunction with either a SEA or a FEM interior fluid. This approach has the advantage of being fast to compute. Once both component of turbulent flow are extracted, the wind noise contribution to interior SPL is computed in minutes. The model setup is also fast, using either a single cavity model or a full vehicle coarse SEA model for target setting of different sub-assembly or a detailed full vehicle SEA model if one is available. Interior SPL predictions are averaged over a volume around the passenger's head unless a FEM cavity is used, then a specific microphone location can be predicted but this only at frequencies below coincidence frequency as mentioned earlier. Finally, using CFD incompressible removes the burden of having to transport the acoustic waves inside the CFD simulation. This simplifies the otherwise complex CFD model setup needed for compressible simulation.

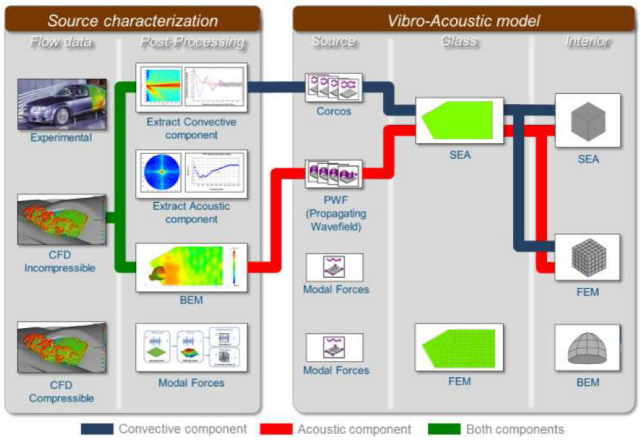


Figure 18. Using CFD incompressible data and a SEA or FE/SEA model to predict interior wind noise

Drawbacks to this approach are that a CFD incompressible flow data is needed which can take several days to run. In this approach, an additional exterior BEM model is needed to characterize the acoustic component. The BEM computation can take several days.

### *FEM Side Glass Approach*

Figure 19 shows the case where the modal forces are used to represent the turbulent flow and a FEM side glass is used in conjunction with a BEM, a FEM or SEA interior fluid. This approach has the advantage of being accurate since the convective source data is taken as is, converted into modal forces, applied on a FEM panel and a deterministic interior fluid can be used. The acoustic component uses the Curle's integral formulation of Lighthill,

therefore an approximation is done on this acoustic component. The contribution to interior noise of the convective and acoustic component is possible with this approach. A SEA interior fluid cavity can also be used to increase frequency range of computation to higher frequencies than the glass coincidence and reduce computation time. The model setup is simple and can be completed within a few hours.

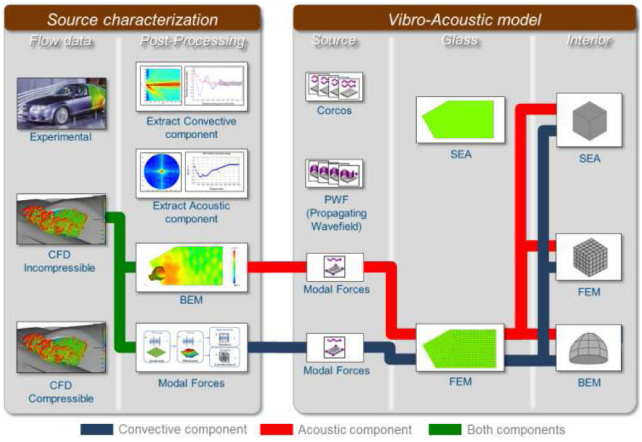


Figure 19. Using CFD incompressible data and a BEM or FEM or FE/SEA model to predict interior wind noise

Drawbacks to this approach are that a CFD incompressible flow data is needed which can take several days to run. In this approach, an additional exterior BEM model is needed to characterize the acoustic component. The BEM computation can take several days.

## CFD Compressible Flow Data Available

### *SEA Side Glass Approach*

When CFD compressible turbulent flow data are available, several approaches can be selected to predict interior vehicle SPL. Figure 20 shows the case where the convective component is extracted from the data to find the Corcos parameters. It also shows that the acoustic component can be evaluated using the 2D wavenumber transform described earlier. Finally, a SEA side glass is used in conjunction with either a SEA or a FEM interior fluid. This approach has the advantage of being fast to compute. Once both component of turbulent flow are extracted, the wind noise contribution to interior SPL is computed in minutes. The model setup is also fast, using either a single cavity model or a full vehicle coarse SEA model for target setting of different sub-assembly or a detailed full vehicle SEA model if one is available. Interior SPL predictions are averaged over a volume around the passenger's head unless a FEM cavity is used, then a specific microphone location can be predicted but this only at frequencies below coincidence frequency as mentioned earlier.

Drawbacks to this approach are that a CFD compressible flow data is needed which can take several days to run. The complex CFD model setup needed for compressible simulation should not be neglected; getting the acoustic waves to properly travel in the CFD fluid is not an easy task.

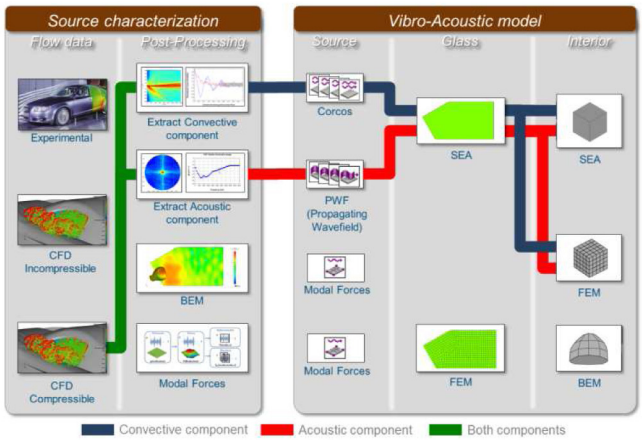


Figure 20. Using CFD compressible data and a SEA or FE/SEA model to predict interior wind noise

### *FEM Side Glass Approach*

Figure 21 shows the case where the modal forces are used to represent the turbulent flow and a FEM side glass is used in conjunction with a BEM, a FEM or SEA interior fluid. This approach has the advantage of being accurate, provided that the source data is accurate, since the CFD source data is taken as is, converted into modal forces, applied on a FEM panel and a deterministic interior fluid can be used. A SEA interior fluid cavity can also be used to increase frequency range of computation to higher frequencies than the glass coincidence and therefore reduce computation time. The model setup is simple and can be completed in a few hours.

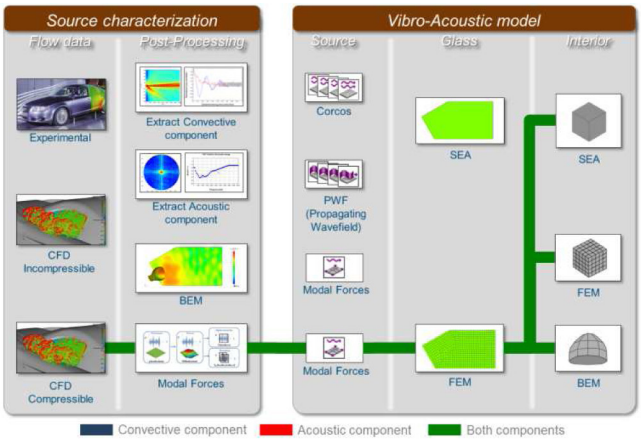


Figure 21. Using CFD compressible data and a BEM or FEM or FE/SEA model to predict interior wind noise

Drawbacks to this approach are that a CFD compressible flow data is needed which can take several days to run. The contribution from the convective and acoustic component cannot be separately computed. This computation can take several days to run if BEM or FEM is used to model the vehicle interior.

## The Right Model at the Right Time

Design decisions are based on information and simulation models available at a certain time. These vary greatly if one is at an early stage of product design or at a validation phase. Figure 22 illustrates a product design process and where the approaches described in previous sections can be used. At an early stage, the side glass SEA based approaches are to be favored since the computation time is

short and trends can be rapidly identified for a specific design (see approaches 1,2,3 in Figure 22). If actual turbulent flow source data is not available yet, the convective and acoustic parameters can always be replaced with the ones from a predecessor vehicle and an early stage computation can be readily available in minutes. The experimental flow source is placed further down the design process since the availability of a prototype comes only at a later stage and only a limited set of measurement can be done on a clay model. Later in the design process, more accurate and computationally demanding approaches can be used such as 4,5 and 6 in Figure 22. These are based on side glass FEM modelling and require much longer run time providing an answer several weeks after the start of the CFD and AVA model building.

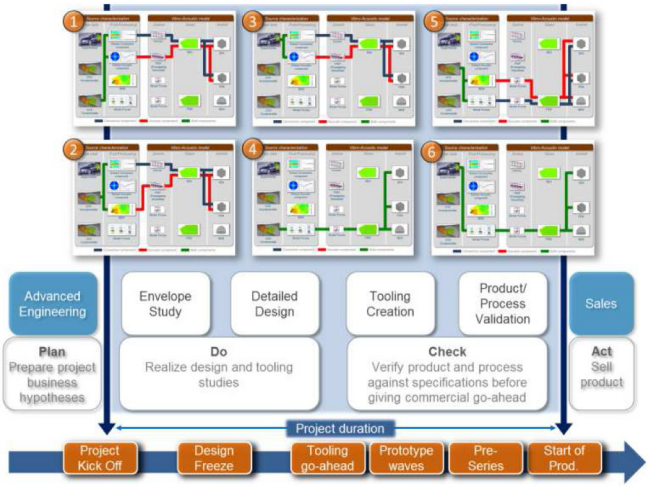


Figure 22. Various approaches for various design process stages. SEA modelling preferred at early stages and deterministic combined with measurements for final verification stages.

It is difficult to categorize the approaches above since the SEA based approaches could also be used for design optimization of A-Pillar and mirror shapes. Once a few design iterations have been pre-selected using CFD-SEA, one could validate the best solution with a more accurate approach before test data is even available. The approaches described here provide flexibility to the user and allow him to select the methods best suited to efficiently answer a question on design change.

## Vibro-Acoustic (VA) Validation

In order to experimentally validate some of these aero-vibro-acoustic approaches to ensure an accurate prediction of interior SPL contribution from wind noise, one must first validate the vibroacoustic models with ideal sources. The objective is to confirm that the vibro-acoustic model can properly represent the behaviour of the vehicle under controlled acoustic excitation before starting to use turbulent flow source data. This section describes the vibro-acoustic validation performed in a semi-anechoic room. The last section of this paper presents the validation of aero-vibro-acoustic models using wind tunnel measurements. These two sections have been done in collaboration with the CAA German Working Group (Audi, Daimler, Porsche and VW) and are based on test campaigns published in 2012 [6].

### *Description of VA Validation Cases*

#### Description of the SAE Body

The SAE body is a generic vehicle model based on the SAE Type 4 (fullback). It is built out of stiff foam and is designed to be used in the current wind noise study which includes acoustic measurements in the cabin, leading to the following requirements of the physical model:

- The noise transmission into the cabin interior needed to be reduced to one relevant acoustic transfer path through the left front side window. This reduces the problem encountered as much as possible when comparing experimental and simulation results.
- The flow over the A-pillar and rear view mirror region, which causes the aero-acoustic excitation of the side window, should be similar to a real car
- Variability of the aero-acoustic excitation by changing components as well as the possibility to modify the acoustic transfer properties of the side window
- A quick set-up of modifications and variants to save time during the wind-tunnel measurement

For more information on the SAE body, please refer to [6]. Figure 23 and Figure 24 show the SAE body geometry, the side mirror, side glass and a view of the thickness of the walls.

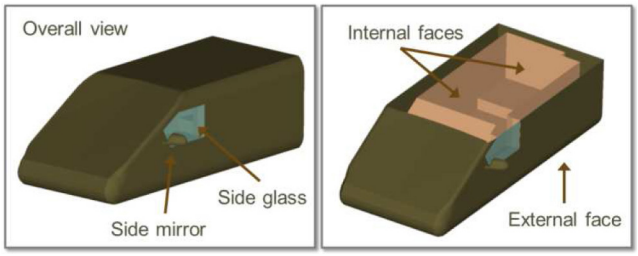


Figure 23. SAE body description: Note the generic shape, the side mirror, side glass, outer and inner faces.

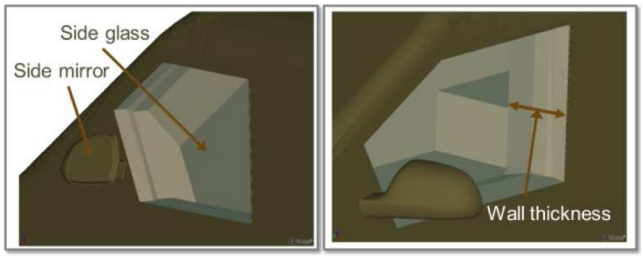


Figure 24. SAE body is quite thick, side glass is mounted flush to outer face

#### Measurement Campaign

For the validation of the vibro-acoustic model, an omnisource was used to generate a sound field either inside or outside the SAE body (Figure 25 showing the inside configuration). A microphone inside the omnisource measured SPL at source location during testing. A set of 5 microphones were placed inside the SAE body to measure the SPL at each location.

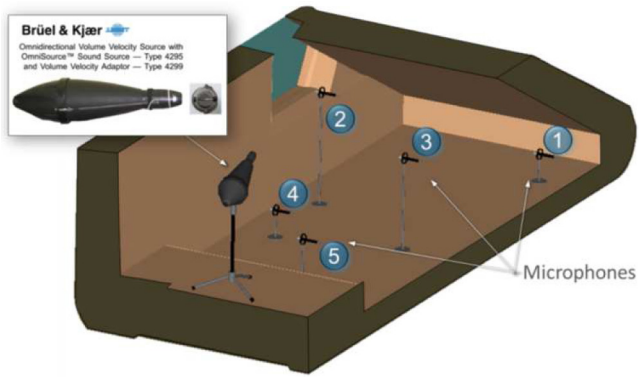


Figure 25. An omnisource is located inside the SAE body along with five randomly located microphones

The measurements campaign used for validation of the vibro-acoustic (VA) model can be split in two groups: i) measurements with the acoustic source inside the SAE body and ii) measurements with the acoustic source outside the SAE body. The first group aims at validating the VA model to ensure that for a given acoustic field inside the SAE body, the VA model can accurately predict the SPL at the five interior microphones (therefore validating the omnisource BEM model) and the exterior acoustic power radiated by the side glass (see figure 26).

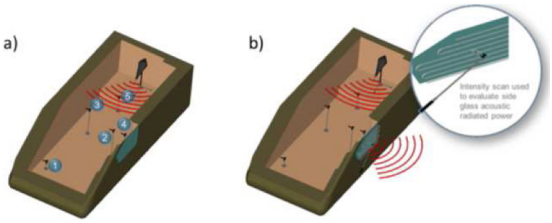


Figure 26. Measurement campaign group where source is located inside SAE body: i) Validation of omnisource BEM model and ii) Validation of sound power radiated by side glass

The second group of measurements aims at validating that for a given exterior point source located at one meter away and at a given angle from the glass, the VA model can properly predict the SPL at each interior microphone. Measurements for 0°, −45° and −90° angles are used to compare with VA model predictions (see figure 27). This configuration is close to the real wind noise transmission mechanism and the accuracy of the final wind noise interior contribution will greatly depend on the ability of the VA model to accurately represent this transmission path.

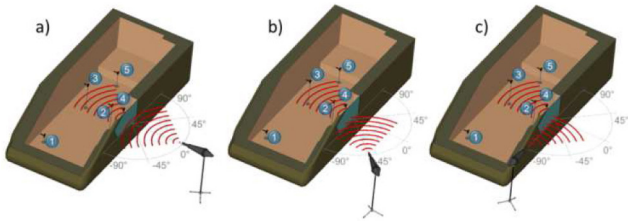


Figure 27. Measurement campaign group where source is located outside SAE body: i) Validation of transmission path between acoustic field with specific headings and interior of SAE body

Finally, to assess the NR of side glass and the different walls, a set of seven patches were defined. Figure 28 shows the patches where average exterior SPL was measured close to the surface of each wall when the omnisource was located inside the SAE body.

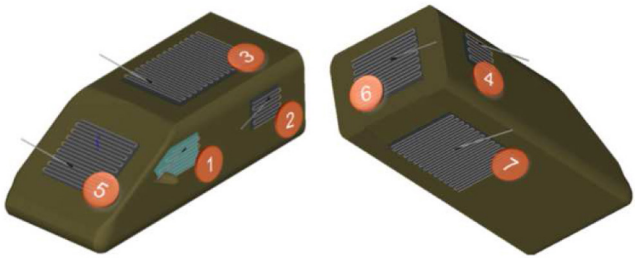


Figure 28. Noise reduction (NR) patches where average SPL is measured.

Figure 29 shows the actual SAE body in the semi-anechoic room where measurements were performed (left) and how the scanning was done (right).


Figure 29. Noise Reduction (NR) measurements performed on several patches around the SAE body.

The results shown in Figure 30 indicate that below 400 Hz, the wall NRs are comparable to the side glass NR. This suggests that care must be taken when interpreting the results in this frequency domain since energy might actually be transferred not only through the side glass but also through the walls. At higher frequencies, only the rear panel exhibit a low NR compared to the glass. This is considered less roblematic since the rear panel is far away from the side glass.

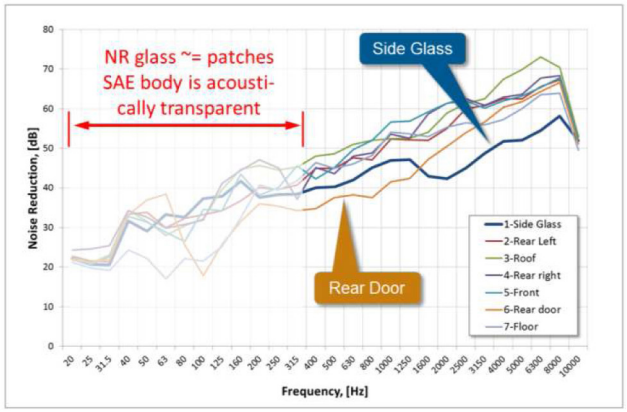


Figure 30. Noise Reduction (NR) results. Starting at 400 Hz, the SAE body patches offer a NR that is higher than the side glass. Below 400 Hz, patches are acoustically as transparent as the side glass.

Test results show that NR SAE body roof, wall and floor are on average 10 dB higher than the side glass at frequency higher than 400 Hz. Region of interest around glass resonance frequency (~3 kHz) show higher NR differences between side glass and other patches. It is therefore considered acceptable to model the walls of the SAE body as rigid and focus in frequency range higher than 400 Hz.

## VA Simulation Models

Since the objective of this study is to characterize the wind noise contribution to interior noise with a high level of accuracy, a BEM model is used for this purpose. The BEM model consists of an interior bounded fluid with rigid walls and an exterior unbounded domain around the SAE body (Figure 31). The omnisource is explicitly modeled based on [23,24] and placed at the same position as in the experimental configuration. The measured SPL inside the omnisource is used as a constraint on a flat rigid surface inside the BEM omnisource model.

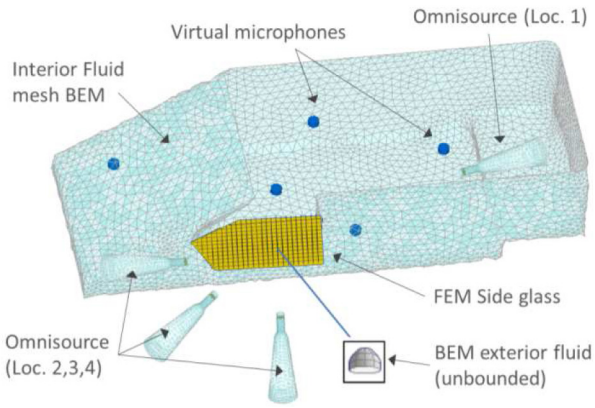


Figure 31. BEM model includes interior and exterior BEM fluid, a FEM glass and the omnisource at various locations

The side glass is represented in FEM and the properties listed in table 2 were used. Computation were made for various boundary condition of the glass and simply supported provided the best correlation with the measurements at low frequencies. It had no impact at frequencies higher than 300 Hz.

Table 2. Side glass structural properties

| Property | Value |
|---|---|
| Glass type | Tempered glass |
| Young's Modulus (E) | 70 GPa |
| Density (Rho) | 2700 Kg/m3 |
| Poisson's Ratio (nu) | 0.33 |
| FEM Boundary Conditions | Simply supported |

The damping loss factor (DLF) of the glass and the interior fluid were measured and used in the simulation (figure 32). At lower frequencies, the DLFs were extrapolated keeping approximately the same slope as the measurements. It is considered overestimated but since it tends to compensate for the fact that the walls are acoustically more transparent at these frequencies, it was decided to keep these values.

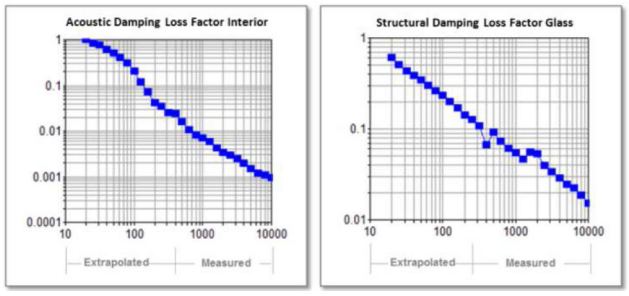


Figure 32. Acoustic and structural DLF used

An additional VA model was built using SEA to compare accuracy and computation time for the case where the source is located inside and the VA models predict the exterior sound power radiated by the side glass. The SEA model includes a SEA acoustic interior fluid, a SEA structural side glass, an area junction and a Semi-Infinite Fluid (SIF) which represent a free field termination. The source in the SEA model is a SPL constraint using the measured average interior SPL. (see figure 33).

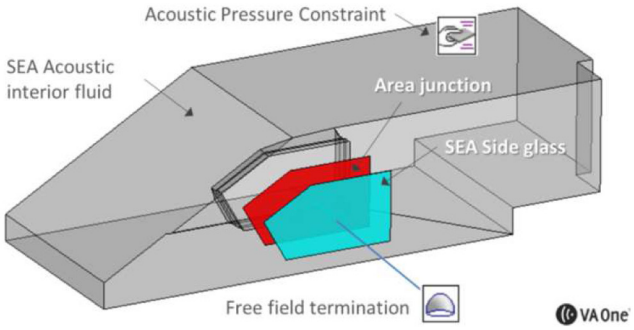


Figure 33. SEA model includes a SEA representation of the interior fluid, the side glass and an anechoic termination representing the exterior of the SAE body

## *Omnisource inside SAE Body*

For VA validation, the omnisource was placed inside the SAE body and prediction were compared with measurement for i) SPL at interior microphone locations and ii) side glass external acoustic power radiation.

### Interior SPL at Microphone Locations

Figure 34 shows comparison of measurements with BEM predictions of SPL at microphones locations and the average levels. At lower frequency, difference between simulation and test can be explained by the fact that in the simulation, the SAE body walls are considered rigid. In reality, there is energy dissipated within the walls and energy transmitted outside through each wall. It also shows at higher frequencies that SPL can be predicted with reasonable accuracy suggesting that the Omnisource BEM model is acceptable.

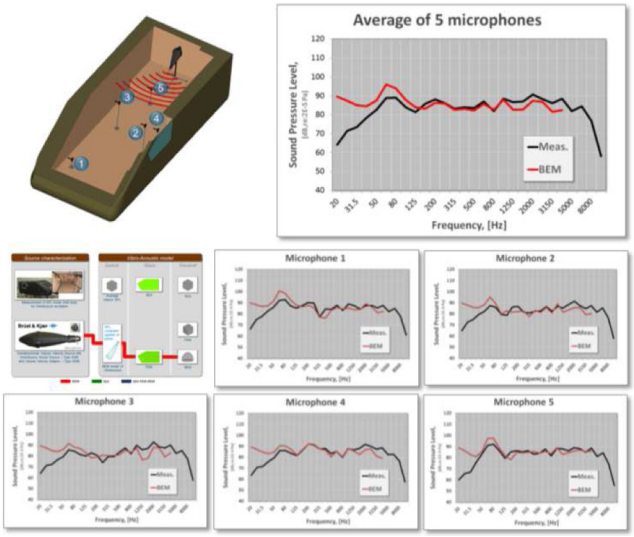


Figure 34. Predicting SPL inside SAE body generated by an omnisource inside

### Acoustic Sound Power Radiated by Side Glass

Figure 35 shows that the acoustic power radiated by the side glass is predicted with high accuracy using either BEM or a pure SEA approach. For SEA, prediction has been done up to 10 kHz in a few seconds with a very high level of accuracy as frequency increases.

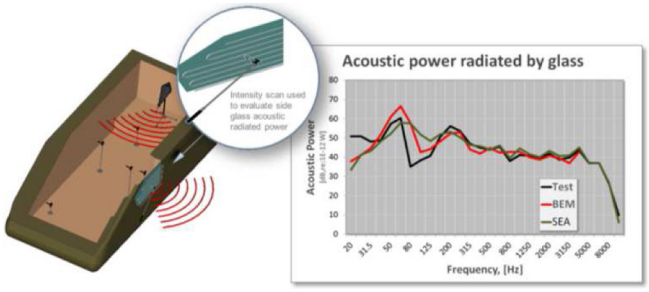


Figure 35. Radiated acoustic power from side glass. Both SEA and BEM are accurate and SEA is computed up to 10 kHz in seconds

## *Omnisource outside SAE Body*

The omnisource was placed outside the SAE body and predictions and measurements were compared for SPL inside the SAE body. Figure 36 shows results for the case where the omnisource is placed at 1 meter and 0° from the side glass normal vector. Correlation levels are very high and one can note that even below 400 Hz, the measured and predicted levels are quite similar. This can be explained by the fact that any acoustic energy entering the SAE body interior through the walls from the source side can easily exit through any other sides since the walls are acoustically transparent compared with the side glass at these low frequencies.

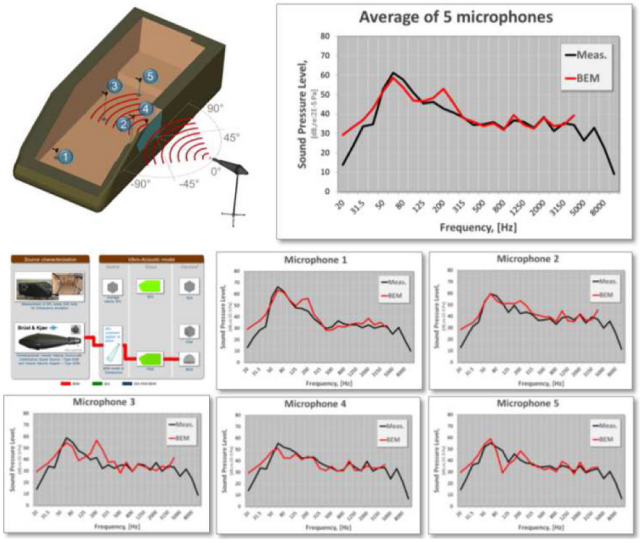


Figure 36. Predicting SPL inside SAE body for an omnisource outside at 0°.

Figure 37 shows the same level of correlation for the case where the omnisource is placed at 1 meter and −45° from the side glass normal.

Figure 38 shows the same level of correlation for the case where source is placed at 1 meter and −90° from the side glass normal. Note that the character of the response is quite different from one location of the source to the other and that the BEM model can properly track the changes in response. Note the 15 dB variation from one angle to the next which is also captured by the BEM model. This is quite comforting since this is a configuration very similar to the real life case where the acoustic waves are believed to come from the front of the side glass where the mirror and A-Pillar are located.

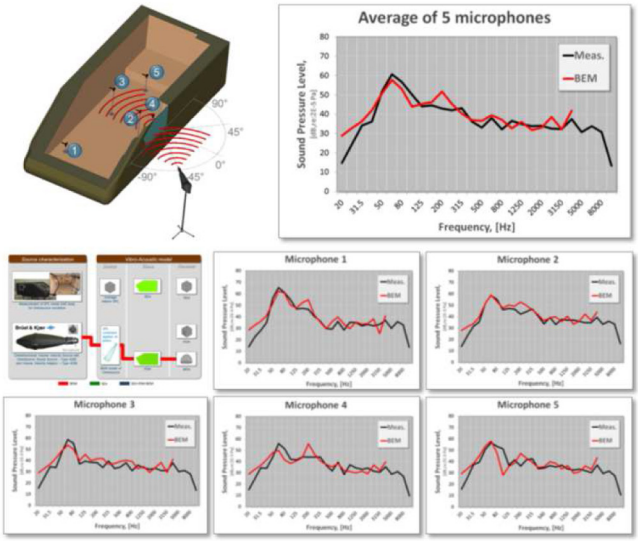


Figure 37. Predicting SPL inside SAE body for an omnisource outside at −45°.

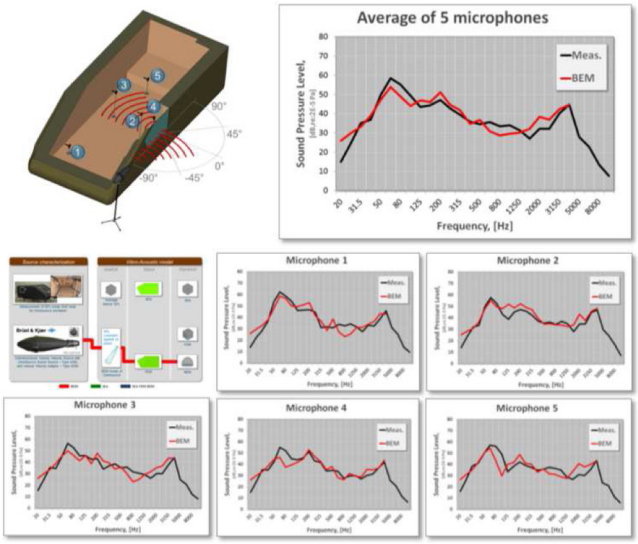


Figure 38. Predicting SPL inside SAE body for an omnisource outside at −90°.

## *Validation of Aero-Vibro-Acoustic Models*

### Experimental Setup

The measurements are described in details in [6]. Figure 39 shows on the left the SAE body in the wind tunnel for the configuration where the vibrations on side glass and SPL inside the SAE body are measured. The right side of the figure shows the surface mounted microphones used to measure the fluctuating surface pressure at the location of the side glass.

Figure 40 shows in more details the microphones used to measure the fluctuating surface pressure.


Figure 39. Wind-tunnel test: (a) glass module, (b) sensor module

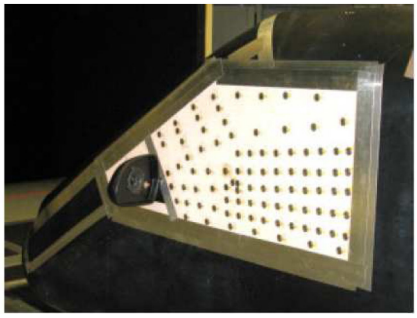

Figure 40. Surface microphones over side glass area.

## CFD Data

The CFD data used for the prediction of wind noise inside the SAE body is the following:

- StarCCM+ Version 6.06.017
- Half model of an SAE body, a very basic car shape on struts, with a rear mirror
- Model size: ~45 million fluid cells
- Compressible Detached Eddy Simulation (DES) based on Spalart-Allmaras (S-A)
- Δt CFD = 2E-05s
- First 0.1s of simulated physical time has been cut away: spurious transition phenomena when starting a transient computation based on steady state results

The pressure time history data was imported into the commercial vibro-acoustics software in [11].

## Aero-Vibro-Acoustic (AVA) models

Figure 41 shows the SEA model containing a SEA side glass structural panel, an area junction and a SEA interior fluid. The sources representing the turbulent flow fluctuating pressures are divided into a convective component (Corcos) and an acoustic component (PWF). Source levels and parameters were extracted from the CFD data based on earlier sections. This model runs in seconds.

Figure 42 shows the FE/SEA Coupled model containing a FEM side glass structural panel, an area junction and a SEA interior fluid. The FE/SEA method has been widely used in various industries over the past 10 years. An introduction to FE/SEA Coupled can be found in [25] and detailed theory in [26,27]. The source representing the turbulent flow is a time domain Fluctuating Surface Pressure (FSP) where the time domain CFD data is converted into frequency domain modal forces as described in an earlier section.

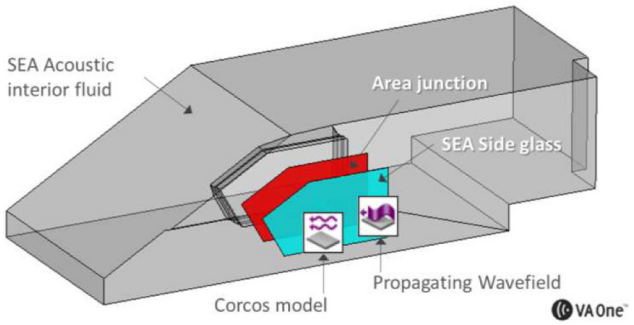


Figure 41. SEA model including SEA interior fluid, SEA side glass panel, area junction and wind noise sources.

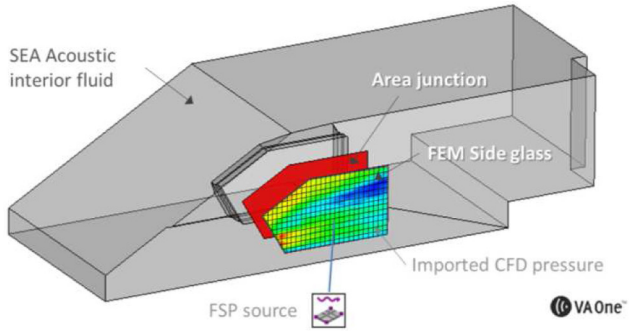


Figure 42. FE/SEA Coupled model including interior SEA fluid, FEM side glass panel, area junction and time domain wind noise source.

Figure 43 shows the BEM model. For clarity, a mesh with coarse element size was used to generate the image but of course a smaller element size is needed to compute to higher frequencies. The mesh size for both the BEM fluid and the structural FEM panel follows the 6 elements per wavelength criteria. The BEM mesh allows for the prediction of SPL at any location inside and outside the SAE body. Five virtual microphones were located at the same location as in the measurements. A time domain FSP (Fluctuating Surface Pressure) source is connected to the side glass to allow the CFD data to be read in the model and converted into frequency domain modal forces as described in an earlier section. Imported CFD pressure data can be visualized as a contour plot in the current frequency domain set in the BEM model as shown in figure 43.

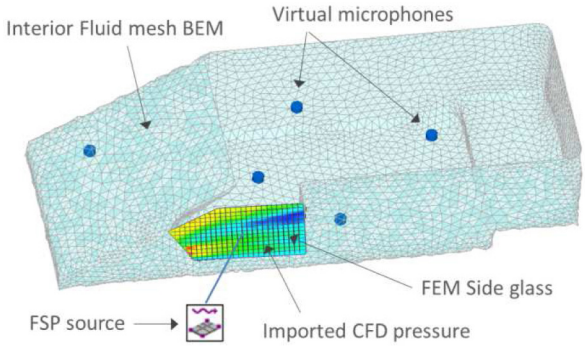


Figure 43. BEM model including FEM side glass, BEM interior fluid and a wind noise (FSP) source.

## AVA Validation Results

The following results are only presented as illustration of correlation accuracy that has been achieved so far on a few configurations. It does not constitute a recommendation of preferred approaches but the status of the current study and merely an indication of what are the next results that will be published at a later time.

Figure 44 shows the average SPL inside the SAE body generated by a 140 km/h wind and the presence of a side mirror predicted using the SEA model. The average SPL is a combination of the convective and acoustic component where the convective contributes at lower frequency and the acoustic at higher frequency. Results are presented in 1/12$^{th}$ octave. One can note that at higher frequencies, the response from a single Propagating Wave Field (PWF) underpredicts the response. Previous experience has shown that using a Diffuse Acoustic Fields (DAF) overpredicts the response and clearly do not properly represent the acoustic component's wave propagation since it assumes that waves have the same probability of hitting the side glass from any angles. The use of 5 PWF on the side glass already improves the correlation with measurements. Further studies are underway to understand how to best model the acoustic component.

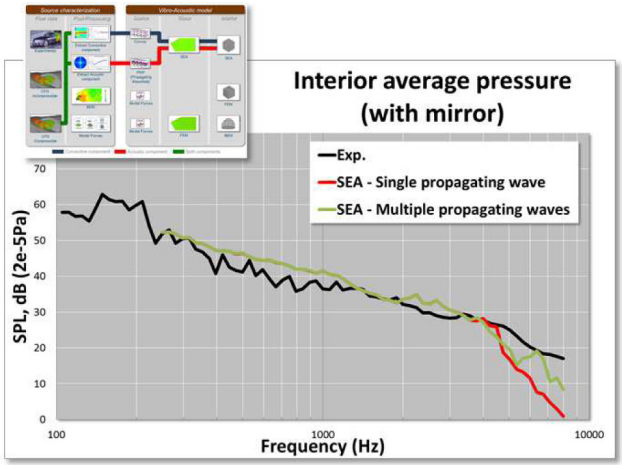


Figure 44. Average SPL inside SAE body generated by 140 km/h wind predicted using a SEA model.

Figure 45 shows the average SPL inside SAE body generated by a 140 km/h wind and the presence of a side mirror predicted using the FE/SEA Coupled model.

The modal forces approach was used. The level of correlation between the measurement and the predicted level is very high. This modelling approach offers a nice alternative to SEA since accuracy is higher and only the side glass has to be modelled in FEM. The use of modal forces provides a better representation of the excitation over the whole side glass area. Computation time is of course large than with SEA since the time domain CFD data has to be processed and the modal basis of the side glass computed and used in the coupled computation. Figure 46 shows the correlation between measurements and the BEM model in 1/12$^{th}$ octave. The modal forces approach was used. The correlation level is higher than the two previous approaches thanks to the BEM representation of the interior fluid.

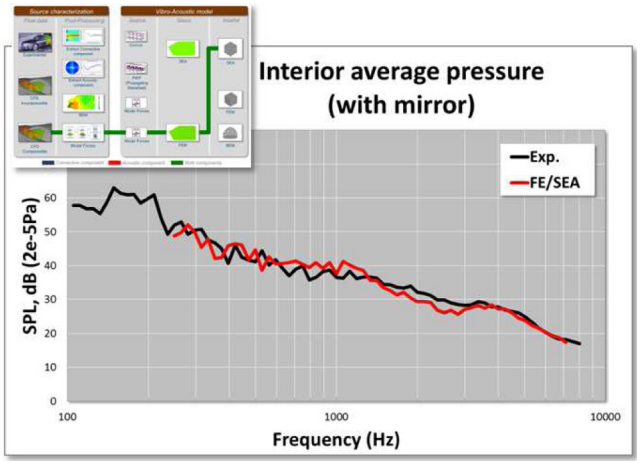


Figure 45. Average SPL inside SAE body generated by 140 km/h wind predicted using a FE/SEA Coupled model.

The BEM approach can also compute SPL at specific microphone locations. Note that each microphone shows the same level of correlation as the average does. This further confirms that the CFD results and the VA model are quite accurate since the AVA model yield such a level of correlation. All BEM computation are shown until a little over 2000 Hz due to the computational expense. Further computation result with a HPC version to increase upper frequency limit will be published as they become available.

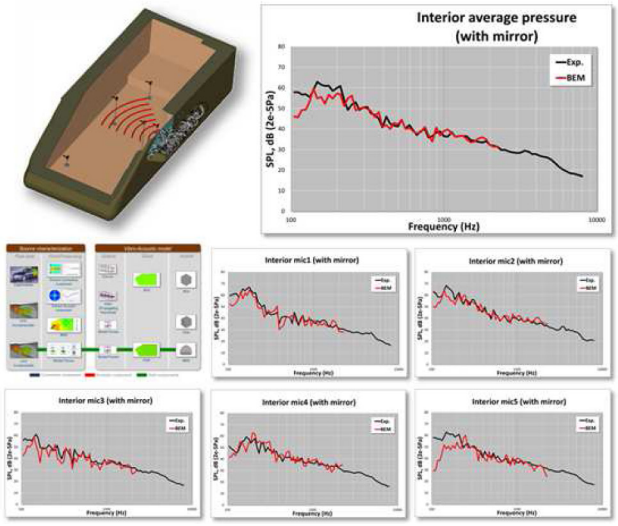


Figure 46. Average and single microphone SPL inside SAE body generated by 140 km/h wind predicted using a BEM model.

It is also interesting to look at the same data in different frequency ranges. Figure 47 shows the data in 1/3$^{rd}$ octave bands and 10Hz constant bandwidth. The 1/3$^{rd}$ octave band results show a difference of only a few dBs at frequencies higher than 300 Hz. The 10 Hz bandwidth shows the character of the response in more details.

It can be seen that the predicted response has a more peaky character. This is explained by the fact that the measurements were averaged over a period of 30 seconds as opposed to the CFD data which was computed for less than 0.5 seconds. One should also note that the conversion of the time signal into frequency domain was done in a deterministic way; the time signal was not averaged and no overlapping windows were used, the whole time period available was directly converted into the frequency domain.

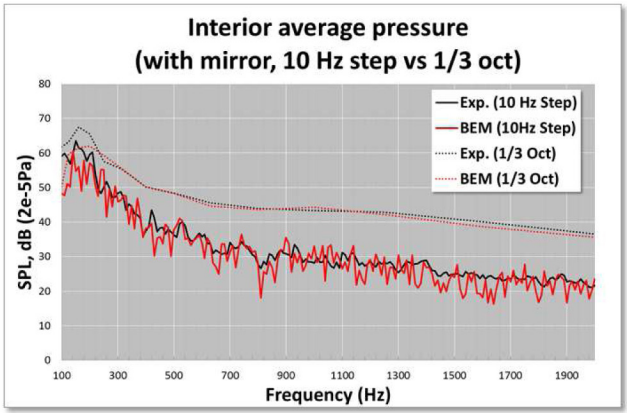


Figure 47. Average SPL inside SAE body generated by 140 km/h wind predicted using a BEM model in 1/3rd octave and 10 Hz frequency step resolution

Figure 48 compares the correlation level between measurements and predicted averaged SPL levels for the cases with and without side rear view mirror in 1/12th octave bands. The results for the case with mirror are reproduced in this graph to compare with the case without mirror. The case without mirror shows a reduction of interior noise of approximately 5 dB over the whole frequency range.

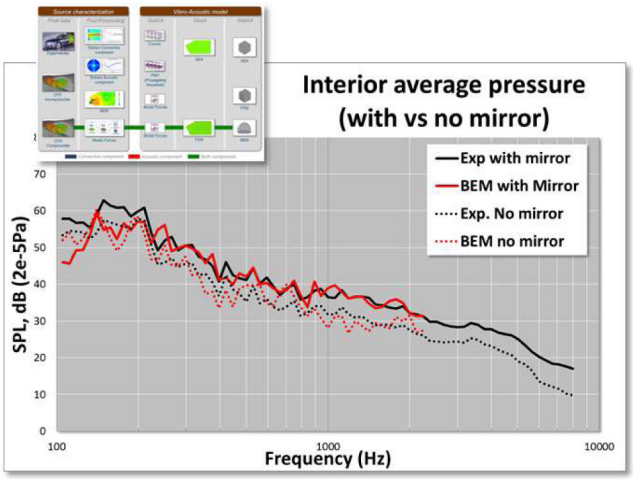


Figure 48. Average SPL inside SAE body generated by 140 km/h wind predicted using a BEM model in 1/12th octave band.

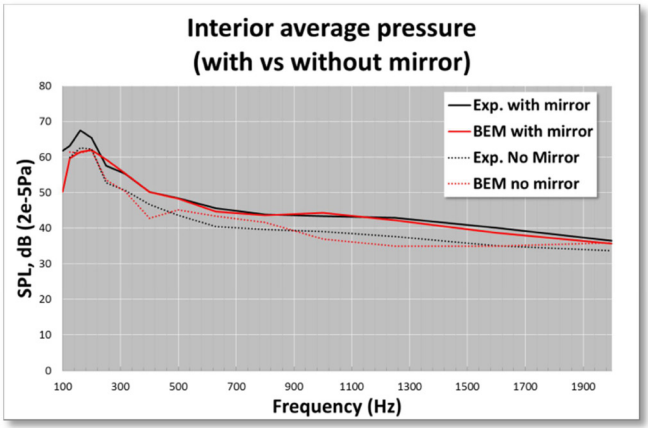


Figure 49. Average SPL inside SAE body generated by 140 km/h wind predicted using a BEM model in 1/3rd octave band.

The predicted levels clearly show the same reduction trend and when the results are shown in 1/3rd octave bands, the response without mirror is within ± 3dB from measurements (Figure 49).

## Conclusion

This paper has presented an overview of available methods for characterizing windnoise sources using various approaches. The advantage and disadvantages of these approaches have been discussed and recommendations have been made in relation to when and with which input data these approaches can be the most efficiently used. The validation exercise of the vibro-acoustic model with test data from the SAE body has shown a high degree of correlation confirming that the vibro-acoustic mechanisms are well modelled. The Aero-Vibro-Acoustics correlation results show a high level of accuracy for the case with and without mirror and confirm that today's approaches can be used for design changes since the underlying physics are well represented by the CFD, VA and AVA models. Results for higher frequencies will be published as they become available.

## References

1. Langley, R., S., “Aero-Vibro-Acoustics: brief review of the theory adopted in VA One”, AVA Special Interest Group, 2012, Düsseldorf, Germany.
2. DeJong, R., Bharj, T., and Lee, J., “Vehicle Wind Noise Analysis Using a SEA Model with Measured Source Levels,” SAE Technical Paper 2001-01-1629, 2001, doi:10.4271/2001-01-1629.
3. DeJong, R., Bharj, T., and Booz, G., “Validation of SEA Wind Noise Model for a Design Change,” SAE Technical Paper 2003-01-1552, 2003, doi:10.4271/2003-01-1552.
4. Peng, G., “SEA Modeling of Vehicle Wind Noise and Load Case Representation,” SAE Technical Paper 2007-01-2304, 2007, doi:10.4271/2007-01-2304.
5. Kralicek, J., Blanchet, D., “Windnoise: Coupling Wind Tunnel Test Data or CFD Simulation to Full Vehicle Vibro-Acoustic Models”, DAGA, Düsseldorf, Germany, 2011.
6. Hartmann, M., Ocker, J., Lemke, T., Mutzke, A. et al., “Wind Noise caused by the A-pillar and the Side Mirror flow of a Generic Vehicle Model”, 18th AIAA/CEAS Aeroacoustics Conference, Paper 2012-2205, Colorado Springs, USA, 2012.
7. Arguillat, B., Ricot, D., Bailly, C., Robert, G., “Measured wavenumber: Frequency spectrum associated with acoustic and aerodynamic wall pressure fluctuations”. JASA 128(4), 2010.
8. Shorter, P., Blanchet, D., and Cotoni, V., “Modeling Interior Noise due to Fluctuating Surface Pressures from Exterior flows,” SAE Technical Paper 2012-01-1551, 2012, doi:10.4271/2012-01-1551.
9. Shorter, P., Cotoni, V., Blanchet, D., “Modeling interior noise due to fluctuating surface pressures from exterior flows”, ISMA, Leuven, Belgium, 2012.
10. Bremner, P., Wilby, J., “Aero-Vibro-Acoustics: Problem Statement And Methods For Simulation-Based Design Solution”, Proc. 8th AIAA/CEAS Aeroacoustics Conference, 2002.
11. VA One 2014, The ESI Group. http://www.esi-group.com
12. Cook, R., et al “Measurement of correlation coefficients in reverberant sound fields”, JASA, 27(6), 1955.

13. Cockburn, J.A., Robertson, J.E., “Vibration Response of Spacecraft Shrouds to In-flight Fluctuating Pressures”, Journal of Sound and Vibration, 1974, 33(4), 399-425.
14. Larko, J.M., Hughes, W.O., “Initial Assessment of the Ares I-X Launch Vehicle Upper Stage to Vibroacoustic Flight Environments”, NASA Technical Memorandum-2008-215167
15. Potschka, N., Callsen, S., “Vibro-acoustic description of a stiffened aircraft structure in flight condition”, ESI Group Vibro-Acoustic User's Conference (VAUC), Düsseldorf, Germany, 2012.
16. Orrenius, U., Cotoni, V., Wareing, A., “Analysis of sound transmission through aircraft fuselages excited by turbulent boundary layer or diffuse acoustic pressure fields”, Internoise, Ottawa, Canada, 2009.
17. Davis, E.B., “By Air by SEA”, Noise-Con, Baltimore, USA, 2004
18. Bremner, P. and Zhu, M., “Recent Progress using SEA and CFD to Predict Interior Wind Noise,” SAE Technical Paper 2003-01-1705, 2003, doi:10.4271/2003-01-1705.
19. Hekmati, A., Ricot, D., Druault, P., “Vibroacoustic behavior of a plate excited by syntesized aeroacoustic pressure fileds”, Proc. 16th AIAA/SEAS Aeroacoustics Conference, AIAA 2010-3950, 2010.
20. Businger, A. Eberle, M. “Computation of underbody flow aero-acoustics for a production vehicle”, ESI Group Global Forum, Munich, Germany 2010
21. Jové, J., Guerville, F., Vallespín, A., “Study Of The Aerodynamic Contribution To The High-Speed Train Cabin Internal Noise By Means Of Hybrid Fe-Sea Modeling”, Internoise, Lisbon, Portugal, 2010.
22. Shorter, P.J., Langley, R.S., and Cotoni, V., “Aero-acoustics: brief review of the theory adopted in VA One”, VAUC/AVASIG: Vibro-Acoustic User's Conference & Aero-Vibro-Acoustic Special Interest Group, Düsseldorf, Germany, 2012.
23. Gade, S., Møller, N., Hald, J., Alkestrup, L., “The use of Volume Velocity Source in Transfer Measurements”, Internoise, Prague, Czech Republic, 2004.
24. Luan, Y., Jacobsen, F., “A method of measuring the Green's function in an enclosure”. JASA 123(6), June 2008.
25. Blanchet, D.: “FE/SEA Coupled”, 10 years after first implementation, Aachen Acoustic Colloquium, Aachen, Germany, 2014.
26. Shorter, P.J. and Langley, R.S.: Vibro-acoustic analysis of complex systems, Journal of Sound and Vibration, 2004.
27. Shorter, P.J., and Langley, R.S., “On the reciprocity relationship between direct field radiation and diffuse reverberant loading”. JASA, 117, 85-95, 2005.

## Contact Information

D. Blanchet
ESI Group
denis.blanchet@esi-group.com

## Acknowledgements

The authors would like to thank the CAA German Working Group composed of Audi, Daimler, Porsche and VW for authorizing ESI to use their experimental and CFD data for the VA and AVA validation work presented in this study. The authors would also like to thank the group for sharing details of the 2D wavenumber decomposition approach the group has commonly agreed to adopt and allowed ESI to implement in its latest version of VA One.

## Definitions/Abbreviations

**SEA** - Statistical Energy Analysis

**BEM** - Boundary Element Method

**FSP** - Fluctuating Surface Pressure: Time domain source type in VA One

**TBL** - Turbulent Boundary Layer: Corcos model of turbulent flow: Frequency domain source in VA One

**PWF** - Propagating wavefield: Waves impinging on a panel at a specific angle: Frequency domain source in VA One

**FEM** - Finite Element Method

**DAF** - Diffuse Acoustic Field: Random incidence wave field: Frequency domain source in VA One

**SPL** - Sound pressure level

**Corcos** - Empirical model describing a complex turbulent flow

**FE/SEA Coupled** - Method that fully couples FEM and SEA in a unique vibro-acoustic model

**VA** - Vibro-Acoustics

**AVA** - Aero-vibro-Acoustics

**TBL** - Turbulent Boundary Layer: Corcos model: Frequency domain source in VA One

**SAE** - Society of Automotive Engineers

**SAE body** - Generic automobile shape

**NR** - Noise Reduction

**CFD** - Computational Fluid Dynamics

**DES** - Detached Eddies Simulation

**CAA** - Computational Aeroacoustics

$\mathbf{k_c}$ - Convective wavenumber, $k_c=\omega/U_c$

$\mathbf{k_o}$ - Acoustic wavenumber, $k_o=\omega/U_o$

$\mathbf{U_c}$ - Convection velocity

$\boldsymbol{\omega}$ - Angular frequency, $\omega = 2\pi f$

The Engineering Meetings Board has approved this paper for publication. It has successfully completed SAE’s peer review process under the supervision of the session organizer. The process requires a minimum of three (3) reviews by industry experts.



ISSN 0148-7191

http://papers.sae.org/2015-01-2326